Neurobiology of Disease

An Acquired Channelopathy Involving Thalamic T-Type Ca^{2+} Channels after Status Epilepticus

John D. Graef,[1,2] Brian K. Nordskog,[1] Walter F. Wiggins,[1] and Dwayne W. Godwin[1,2]

[1]Department of Neurobiology and Anatomy, and [2]The Neuroscience Program, Wake Forest University School of Medicine, Winston-Salem, North Carolina 27157

Some epilepsies are linked to inherited traits, but many appear to arise through acquired alterations in neuronal excitability. Status epilepticus (SE) is associated with numerous changes that promote spontaneous recurrent seizures (SRS), and studies have suggested that hippocampal T-type Ca^{2+} channels underlie increased bursts of activity integral to the generation of these seizures. The thalamus also contributes to epileptogenesis, but no studies have directly assessed channel alterations in the thalamus during SE or subsequent periods of SRS. We therefore investigated longitudinal changes in thalamic T-type channels in a mouse pilocarpine model of epilepsy. T-type channel gene expression was not affected during SE; however $Ca_V3.2$ mRNA was significantly upregulated at both 10 d post-SE (seizure-free period) and 31 d post-SE (SRS-period). Overall T-type current density increased during the SRS period, and the steady-state inactivation shifted from a more hyperpolarized membrane potential during the latent stage, to a more depolarized membrane potential during the SRS period. $Ca_V3.2$ functional involvement was verified with $Ca_V3.2$ inhibitors that reduced the native T-type current in mice 31 d post-SE, but not in controls. Burst discharges of thalamic neurons reflected the changes in whole-cell currents, and we used a computational model to relate changes observed during epileptogenesis to a decreased tendency to burst in the seizure-free period, or an increased tendency to burst during the period of SRS. We conclude that SE produces an acquired channelopathy by inducing long-term alterations in thalamic T-type channels that contribute to characteristic changes in excitability observed during epileptogenesis and SRS.

Introduction

Temporal lobe epilepsy (TLE), the most common and drug-resistant form of adult epilepsy (Morimoto et al., 2004), can arise from a single episode of status epilepticus (SE). It is characterized by limbic seizures that often generalize to other areas, leading to impaired cortical function (Guye et al., 2006). It has been hypothesized that epileptogenesis is produced by an imbalance between glutamatergic excitation and GABAergic inhibition (McNamara, 1994), and several studies have focused on alterations in neuronal excitability (Coulter, 2001; Lothman et al., 1995; Sutula et al., 1989; Bertram et al., 2001).

The intrinsic voltage-dependent properties of neurons are an important determinant of electrical excitability. Several inherited channelopathies are found in human epilepsy (Chen et al., 2003; Khosravani et al., 2004, 2005), yet not all cases can be linked to specific genes (Bernard et al., 2004; Jung et al., 2007; Becker et al., 2008). Studies of T-type Ca^{2+} channels in rodent models of TLE have found an upregulation of T-type current in the dendrites of CA1 hippocampal neurons that corresponds to increased neuronal bursting (Su et al., 2002). Recently, Becker et al. (2008) demonstrated an acute and specific transcriptional upregulation of one T-type isoform, $Ca_V3.2$, in the CA1 region of the hippocampus only a few days after SE. These changes however, had dissipated 3 weeks later, suggesting limited, direct $Ca_V3.2$ involvement in the generation of spontaneous recurrent seizures (SRS), even though $Ca_V3.2$ KO mice showed reduced pathophysiological changes normally associated with epileptogenesis.

In addition to the hippocampus, midline thalamic nuclei (reuniens and rhomboid) also express T-type Ca^{2+} channels (Talley et al., 1999) and are part of the seizure network (Bertram et al., 2008). The reuniens nucleus (RE) is of particular interest because it sends excitatory projections to both the dendritic region of CA1 (Wouterlood et al., 1990) and the entorhinal cortex (Vertes et al., 2006). This places RE in position to modulate the temporoammonic pathway, a set of connections between the entorhinal cortex and CA1 that is dysregulated in animal models of TLE, and therefore implicated in the generation of hippocampal ictal activity (Ang et al., 2006). Investigations involving changes in midline thalamus have demonstrated increased neuronal bursts from rats exhibiting chronic SRS (Bertram et al., 2001), leading to the conclusion that the midline thalamus is an important part of the TLE circuit (Bertram et al., 2008). More importantly, the appearance of increased thalamic bursts were recorded from epileptic rats 2 months after SE, which serves to correlate changes in the physiological properties of midline thalamic neurons with the appearance of SRS.

We sought to determine whether increased thalamic bursts resulting from SE are associated with transcriptional and func-

Received Jan. 13, 2009; revised Feb. 14, 2009; accepted Feb. 17, 2009.

This work was supported by National Institutes of Health Grants F31AA017048, T32AA7565, R21EY018159, R01AA016852, and R01AA015568, Citizens United for Research on Epilepsy, and the Tab Williams Family Fund. We thank Georgia Alexander for critique of this manuscript. We also thank Tiffany Fisher and Emilio Salinas for discussions in the development of an early version of the computational model.

Correspondence should be addressed to Dr. Dwayne W. Godwin, Department of Neurobiology and Anatomy, Wake Forest University School of Medicine, Medical Center Boulevard, Winston-Salem, NC 27127. E-mail: dgodwin@wfubmc.edu.

DOI:10.1523/JNEUROSCI.0198-09.2009

 0270-6474/09/294430-12$15.00/0

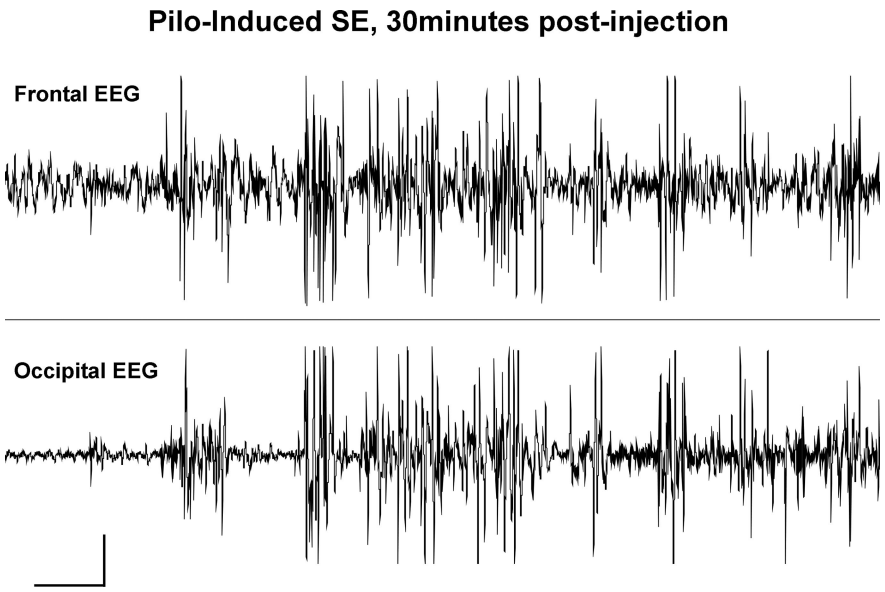

Figure 1. Pilocarpine-induced SE seizure in a C57 mouse. Example surface EEG recordings from mouse frontal cortex (top) and parietal/occipital cortex (bottom) 30 min after pilocarpine injection. Calibration: 200 μV, 10 s.

tional changes in midline thalamic T-type channels. We found that SE increased $Ca_V3.2$ mRNA and altered T-type channel inactivation properties that corresponded to both the decreased tendency to burst during the seizure-free silent period, and the increased tendency to burst during the chronic period of SRS. Our results indicate specific, acquired changes in T-type channel expression and function that are consistent with the appearance of a hyperexcitable population of midline thalamic neurons that could contribute to seizure development and generalization.

Materials and Methods

Animals and experimental design. Mice were prepared according to established protocols (Turski et al., 1983; Shibley and Smith, 2002) and in accord with procedures approved by the Institutional Animal Care and Use Committee of Wake Forest University and in agreement with National Institutes of Health and United States Department of Agriculture guidelines, including measures to eliminate suffering and to reduce animal numbers to a minimum. Briefly, 60 six-week old male C57BL/6 mice (Harlan) were injected with the muscarinic agonist pilocarpine (330 mg/kg, i.p.) a dose which has been shown to reliably induce SE in C57BL/6 mice (Shibley and Smith, 2002; Peng et al., 2004; Winokur et al., 2004). Peripheral muscarinic effects were minimized by prior administration of methyl-scopolamine (1 mg/kg, i.p., 30 min before injecting pilocarpine). 55 of the 60 mice treated with pilocarpine experienced SE as characterized by intense salivation, head tremors, forelimb clonus, rearing and falling. In addition, SE seizures were further verified electrographically in a subset of pilocarpine-injected animals (Fig. 1). Fourteen of the mice that experienced SE (23%) died during the acute post-treatment phase (a rate that is consistent with other reports; Jung et al., 2007). Surviving animals that experienced SE were closely monitored in the lab for 24 h, and were used as the pilo-SE group. Along with the five pilocarpine-injected mice that did not experience SE, an additional cohort of age-matched mice were injected first with methyl-scopolamine, followed 30 min later by a sterile saline injection and used as the control group. Thalamic tissue was harvested at three time points: 4 h postinjection, corresponding to the peak of SE; 10 d postinjection, corresponding to a period after SE and before spontaneously recurrent seizures; and 31 d postinjection, corresponding to the development of spontaneously recurrent seizures. At each analysis time point mice were anesthetized with isoflurane and decapitated for gene expression and electrophysiological experiments.

RNA isolation and real-time reverse transcriptase PCR. After decapitation, the brains were removed and the thalamus and hippocampus were dissected in ice-cold artificial CSF (ACSF) containing (in mM): 124 NaCl, 5 KCl, 2 $MgSO_4$, 2 $CaCl_2$, 23 $NaHCO_3$, 3 NaH_2PO_4, 10 glucose (pH 7.4, osmolarity 290–300 mOsm). After sagittally hemisecting the brain, tissue from hippocampus and midline thalamic nuclei was harvested from the medial surface with a tapered Pasteur pipette. Tissue punches were then frozen in liquid nitrogen and stored at −80°C. After removal from storage, tissue was immediately homogenized in TriREAGENT (Molecular Research Center) using a PowerGen 125 Tissue Homogenizer (Fisher Scientific). Total RNA was isolated as described in the manufacturer's protocols. Absence of DNA contamination was verified in the purified RNA preparation by performing cDNA synthesis in the absence of reverse transcriptase (RT control) followed by RT-PCR (see below). As an added precaution, RNA was further purified using Qiagen RNeasy spin columns (Qiagen) to remove possible contaminants including genomic DNA. RNA concentration was measured using a ND-1000 spectrophotometer (NanoDrop; ThermoFisher Scientific) and quality was assessed by electrophoresis in 1% agarose formaldehyde gels. cDNA was synthesized using the SuperScript III First Strand Synthesis System (Invitrogen) for real-time PCR with random hexamer primers as per manufacturer's instructions. Real-time PCR was performed using the 5′-exonuclease method (Taqman; Applied Biosystems). Taqman Universal PCR Mix (Applied Biosystems) containing *Taq*DNA polymerase, dNTPs (+dUTP), and buffers was used according to manufacturer's directions. Real-time PCR was performed on an ABI 7300 thermal cycler (Applied Biosystems) using 2 ng of sample cDNA amplified as described by Taqman Universal PCR Master Mix (Applied Biosystems) protocols. The cycling parameters were as follows: first 50°C for 4 min followed by DNA polymerase activation step at 95°C for 10 min and a two-temperature PCR of 40 cycles at 95°C for 15 s (denaturing step) followed by 55°C for 1 min (annealing step). GAPDH amplification was the same but the annealing temperature was set at 60°C. Expression levels for the T-type Ca^{2+} channel isoforms and for GAPDH were quantified using the relative standard curve method (Johnson et al., 2000) using dilutions of cDNAs prepared from total RNA isolated from the thalamus of control, saline-injected mice. Standard curves were run on the same plates as the samples to insure that they were directly comparable. Based on the relationship between cycle threshold (C_T) values and nanograms of cDNA contained in the standard curve, a relative nanogram value was determined for each sample. Relative expression of Ca_V3 mRNA shown in Figure 2 was quantified according to the $\Delta\Delta C_t$ method (Livak and Schmittgen, 2001). Each gene/animal was run in duplicate and normalized to GAPDH gene expression. GAPDH was used in our studies as a reference gene because of its stability under a wide range of experimental treatments (Barber et al., 2005). Data are represented as the group mean ± SEM.

Primers and probes. Primers and probes for genes $Ca_V3.1$, $Ca_V3.2$ and $Ca_V3.3$ were designed using PrimerQuest software from Integrated DNA Technologies (IDT) (Nordskog et al., 2006); Primer3 code is available at http://primer3.sourceforge.net/ based on published mouse sequences (GenBank). GAPDH primer and probe sequences were those reported in Nordskog et al. (2006). Care was taken to ensure that the primers and probes were included in all known mouse splice variants for each T-type Ca^{2+} channel. As a further step, the designed mouse primer and probe locations were compared with corresponding regions on human genes to ensure that the locations were included in all known human splice variants. Primer and probe specificity was determined by performing a Blast search using NCBI software (http://blast.ncbi.nlm.nih.gov/Blast.cgi) compared with all published mouse sequences. Primer and probes were synthesized by IDT. Primers were further verified and optimized by run-

ning test samples to ensure the correct amplicon size (as determined by size from the published sequence) was produced after PCR amplification of the target sequence. Amplicons were separated by agarose gel electrophoresis (2% agarose in TAE buffer) and stained with ethidium bromide (Sigma-Aldrich) and visualized using a Gel Doc System (Bio-Rad Laboratories). Only one band corresponding to the predicted amplicon size was detected for each primer set. Probes contained the 5′-fluorescent reporter dye FAM, and the 3′-quencher Iowa Black (IDT). All genes of interest were normalized to GAPDH gene expression because GAPDH possesses stability under a wide range of experimental treatments (Barber et al., 2005; Meldgaard et al., 2006). However, because recent reports have demonstrated that GAPDH may not be stable under some conditions (Schmittgen and Zakrajsek, 2000; Dheda et al., 2004), we verified stable baseline GAPDH levels for all conditions (data not shown).

Slice preparation. In preparation for electrophysiological recordings, after decapitation the brain was rapidly removed and immersed in oxygenated (95% O_2-5% CO_2), ice-cold sucrose substituted ACSF containing (in mM): 220 sucrose, 12 $MgSO_4$, 10 glucose, 2 KCl, 1.5 NaH_2PO_4, 26 $NaHCO_3$, 0.2 $CaCl_2$ (pH 7.4, osmolarity 290–300 mOsm). A block of tissue containing midline thalamic nuclei was sectioned on a vibratome (model OTS 4000; Electron Microscopy Sciences) at 400 μm, and slices were maintained in oxygenated, warm (34°C) ACSF containing (in mM): 124 NaCl, 5 KCl, 2 $MgSO_4$, 2 $CaCl_2$, 23 $NaHCO_3$, 3 NaH_2PO_4, 10 glucose (pH 7.4, osmolarity 290–300 mOsm), for ≥1.5 h before being transferred to a submerged recording chamber for recordings (Harvard Apparatus).

Intracellular recordings. Whole-cell patch clamp recordings of T-type currents were performed according to established protocols (Alexander et al., 2006; Carden et al., 2006) at all time points from which gene expression data were collected. For cells in the 31 d control and 31 d pilo-SE groups, recording were made from neurons from mice 28–33 d after treatment, with the median time point being 31 d postinjection. During recording, thalamic slices were continuously perfused with oxygenated ACSF at a flow rate of 1.5–2 ml/min. Patch pipettes (5–10 MΩ) were pulled from borosilicate glass (Sutter Instruments) with a PC-10 vertical puller (Narishige International USA), and were filled with an internal solution containing (in mM): 100 gluconic acid, 100 CsOH, 10 NaCl, 10 HEPES, 20 TEA-Cl, 1 EGTA, 4 Na-ATP (pH 7.3 with 2N CsOH, osmolarity 270–290 mOsm) for voltage-clamp experiments, and (in mM): 117 K-gluconate, 13 KCl, 1 $MgCl_2$, 0.07 $CaCl_2$, 10 HEPES, 0.1 EGTA, 2 Na-ATP (pH 7.3 with 2 N KOH, osmolarity 270–290 mOsm) for current-clamp experiments. A liquid junction potential of +14 mV for Cs-gluconate-based internal solutions and +13 mV for K-gluconate-based internal solutions, determined experimentally, were corrected for *post hoc*. Cellular activity was acquired with an AxoClamp 2B amplifier and HS-2A headstage (Molecular Devices), digitized with a Digidata 1322 (Molecular Devices), and analyzed using pCLAMP 9.0 software (Molecular Devices). To acquire cells, patch pipettes were advanced "blind" through tissue in bridge (or current clamp) mode until an increase in pipette resistance was observed, indicating the possible presence of a cell. A >1 GΩ seal was then formed, and the membrane was ruptured to allow whole cell access. The access resistance was minimized by applying positive pressure to the pipette, clearing the free ends of the membrane to allow the flow of current. Once a cell had been patched in current clamp mode, the amplifier was then switched to single-electrode voltage clamp recording mode. Neurons were clamped at high gain to eliminate the potential for loss of voltage control. For all voltage-clamp experiments, tetrodotoxin (TTX, 1 μM; Alomone Laboratories) was included in the ACSF to block sodium action potentials. In experiments in which ascorbic acid and Ni^{2+} were used, ascorbate and $NiCl_2$ (Sigma-Aldrich) were dissolved in ACSF (pH 7.4 with NaOH) and introduced into the bath solution at a rate of 0.2 ml/min and 0.04 ml/min respectively. Both input resistance and capacitance were calculated *post hoc* from a 500 ms, −50 mV test potential delivered at the end of each sweep.

Analysis. Average peak activation and inactivation currents were normalized to the peak of the maximally available current (I/I_{max}). This relative current was plotted as a function of prepulse potential and fitted with a Boltzmann equation: $I = I_{max}/(1 + \exp[(V - V_{50})/k])$, to derive, by least-squares fits, the half-maximal voltage (V_{50}) and slope factor (k) values (Coulter et al., 1989; Crunelli et al., 1989). Each recorded current provides a unique Boltzmann fit, and the mean derived V_{50} and k values for all cells in a given cohort were used for comparison between groups. The decay of maximally elicited T-type currents for all voltage-clamp recorded cells were fit in Clampfit 9.0 (Molecular Devices) with a standard exponential decay function,

$$I(t) = \sum_{i=1}^{n} A_i * \exp(-t/\tau_i) + C.$$

Net charge was calculated by integrating the total area of the maximum elicited current deflection for each cell. Significant differences between groups were tested as appropriate with an unpaired *t* test, paired *t* test, or Mann–Whitney test, using Prism 4 (GraphPad Software Inc.) with the significance level set to $p < 0.05$. Data are represented as the group mean ± SEM.

The model. We created custom M-files developed in MATLAB 7.6 to model burst responses elicited by the T-type current under varying conditions for all experimental cohorts. Our model is a modified version of the integrate-and-fire-or-burst (IFB) model constructed by Smith et al. (2000). The equation for this model is $C(dV/dt) = I_{app} - I_L - I_T$.

An action potential was generated when the membrane potential reached a defined threshold (V_Θ), such that $V(t) = V_\Theta \Rightarrow V(t^+) = V_{reset}$.

We then altered the standard parameters and derived additional parameters for the model based on experimental data collected during voltage-clamp experiments. A constant conductance leakage current (I_L), is incorporated in the form $I_L = g_L(V - E_L)$, with g_L being calculated from the input resistance (R_m) and capacitance-derived cell surface area (S_A), using the following equation, $g_L = 1/(R_m * S_A)$. The low-threshold Ca^{2+} current (I_T) is given by $I_T = I_{ratio} g_T m_\infty h(V - E_{Ca})$, with I_{ratio} being the fraction of T-type current available based on empirical steady-state inactivation and activation measurements fitted with a Boltzmann equation, and g_T being the maximal T-type conductance derived from the experimentally determined maximum T-type current (I_{max}) and holding potential (V_{hold}) with the following equation, $g_T = I_{max}(V_{hold} - E_{Ca})$. The equations characterizing the activation (m_∞) and inactivation (h) of I_T were adopted from Smith et al. (2000), with $m = 1$ (if $V > V_h$); $m = 0$ (if $V < V_h$); $dh/dt = -h/\tau_h^-$ (if $V > V_h$); $dh/dt = (1 - h)/\tau_h^+$ (if $V < V_h$).

We then generated contour plots of elicited bursts by running the model at 21 different holding potentials after 21 different hyperpolarizing current injections of 500 ms and plotted the number of action potentials per burst at each of the 441 points. The values for the model parameters are given in Table 1. We then derived a burst index from each plot that was calculated by multiplying the total percentage of elicited bursts by the average number of action potentials per burst.

Table 1. Parameters for the IFB model

Parameter	4 h saline	4 h pilo	10 d saline	10 d pilo	31 d saline	31 d pilo
E_{Ca} (mV)	121.9	121.9	121.9	121.9	121.9	121.9
E_L (mV)	−65.0	−65.0	−65.0	−65.0	−65.0	−65.0
$V_{50_{act}}$ (mV)	−77.4	−76.2	−74.9	−81.7	−75.8	−74.8
k_{act}	2.0	2.0	1.8	2.4	2.1	2.0
$V_{50_{inact}}$ (mV)	−88.3	−85.3	−85.8	−90.8	−86.7	−80.4
k_{inact}	3.5	3.4	4.2	4.8	4.2	4.9
g_{Ca} (mS/cm^2)	0.062	0.057	0.053	0.050	0.049	0.077
g_L (mS/cm^2)	0.093	0.071	0.081	0.065	0.059	0.069
V_Θ (mV)	−40	−40	−40	−40	−40	−40
V_{reset} (mV)	−50	−50	−50	−50	−50	−50
V_h (mV)	−75	−75	−75	−75	−75	−75
τ_h^- (ms)	12.4	12.7	12.5	16.6	12.2	13.9
τ_h^+ (ms)	100	100	100	100	100	100
C_m (μF/cm^2)	1	1	1	1	1	1

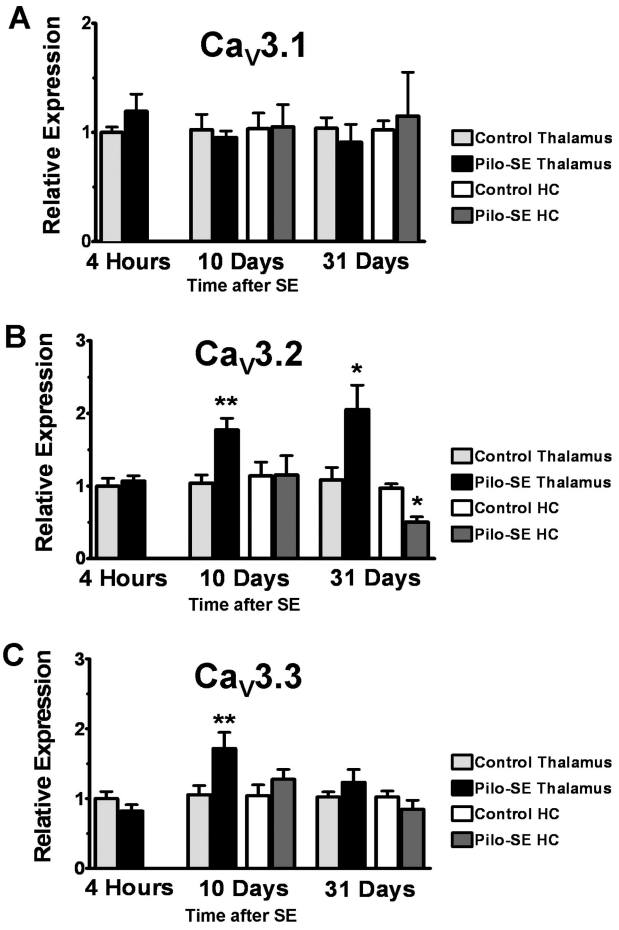

Figure 2. T-type channel gene expression during progression of pilocarpine-induced seizures. Relative mRNA levels for all three Ca_V3 transcripts were determined using real-time RT-PCR and normalized to GAPDH expression. ***A***, No differences in $Ca_V3.1$ expression between controls ($n = 7$) and pilo-SE ($n = 7$) cohorts were seen in either thalamic or hippocampal tissue at all time points after SE. ***B***, At both 10 and 31 d post-SE, pilo-SE mice showed a 1.8-fold ($n = 7$) and 2.1-fold ($n = 7$) increase respectively, compared with controls ($n = 7$ for both control groups; $^*p < 0.05$, $^{**}p < 0.01$, Mann–Whitney test). A significant decrease in $Ca_V3.2$ expression was seen in hippocampal tissue 31 d after SE (2-fold, $n = 7$; $^*p < 0.05$, Mann–Whitney test). ***C***, At 10 d post-SE, $Ca_V3.3$ also showed a significant increase in gene expression (1.7-fold, $n = 7$; $^{**}p < 0.01$, Mann–Whitney test), compared with controls ($n = 7$).

Results

SE alters T-type channel gene expression

We examined T-type Ca^{2+} channel gene expression in cohorts of control, non-SE as well as pilocarpine-injected SE mice from tissue that was harvested at the same three time points (4 h into SE, 10 d post SE and 31 d post SE; corresponding to the time points of the physiological measurements). Based on relative nanogram values obtained from a standard curve, the relative distribution of the three T-type channel isoforms for all cohorts did not change, with $Ca_V3.1 > Ca_V3.2 \sim Ca_V3.3$ for midline thalamic nuclei, and $CaV3.2 > Ca_V3.1 \sim Ca_V3.3$ for hippocampus, regardless of the condition (data not shown), which is consistent with previous studies done in rat (Talley et al., 1999).

We first compared the relative gene expression for all three T-type Ca^{2+} channel isoforms from control and pilo-SE thalamic tissue 4 h postinjection (corresponding to the peak of SE) and found no significant differences for any of the isoforms between the control and pilo-SE groups (Fig. 2).

We then compared thalamic and hippocampal relative gene expression between control and pilo-SE mice 10 d after treatment; a time point that corresponds to a latent, seizure-free period after SE (Shibley and Smith, 2002; Peng et al., 2004; Winokur et al., 2004), but preceding the chronic period of SRS (Fig. 2). A 1.8-fold increase in $Ca_V3.2$ expression (Fig. 2*B*) and a 1.7-fold increase in $Ca_V3.3$ expression (Fig. 2*C*) was seen in thalamic tissue harvested from mice 10 d after SE compared with control thalamic tissues (controls, $n = 7$; pilo-SE, $n = 7$; $p < 0.05$, Mann–Whitney test). However, neither $Ca_V3.2$ nor $Ca_V3.3$ showed increased expression in hippocampal tissue from mice 10 d after SE, which is consistent with previous reports (Becker et al., 2008).

Finally, thalamic and hippocampal Ca_V3 gene expression was also compared between control and pilo-SE tissue that was harvested at 31 d after treatment; a time point after the onset of SE that corresponds to the appearance of SRS (Fig. 2). Only $Ca_V3.2$ showed significant changes in expression levels (2.1-fold increase in thalamus, 2-fold decrease in hippocampus) 31 d after SE (Fig. 2*B*, controls, $n = 7$; pilocarpine, $n = 7$; $p < 0.05$, Mann–Whitney test). These findings illustrate a slowly evolving pattern of regionally specific changes in $Ca_V3.2$ mRNA over the course of pilocarpine-induced epileptogenesis.

SE changes T-type channel functional properties

To determine whether increases in T-type channel gene expression were associated with functional differences in the native current, we characterized whole-cell currents from thalamic relay neurons from brain slices prepared at the relevant time points after treatment. We recorded the T-type Ca^{2+} responses from a total of 101 midline thalamic relay neurons using the whole-cell patch-clamp technique. Of these, 86 were recorded under voltage-clamp conditions, and 15 were recorded under current-clamp conditions. Ca^{2+} currents were recorded in voltage-clamp recording mode with TTX (1 μM) introduced into the ASCF to block voltage-dependent Na^+ currents.

Bursts can be elicited in mouse thalamic relay cells by injecting a hyperpolarizing current pulse into the cell, resulting in the deinactivation of the T-type Ca^{2+} current followed by activation that occurs during repolarization of the membrane (Jahnsen and Llinás, 1984). Using this paradigm, Ca^{2+} currents were recorded and characterized from midline thalamic neurons in both control, non-SE and pilo-SE mice at all three time points, 4 h, 10 d, and 31 d postinjection. Voltage-clamp protocols were used to isolate the low-threshold Ca^{2+} current enabling the measurement of steady-state gating properties. Relevant electrophysiological measurements are shown in Table 2.

Ca^{2+} current amplitude and density

Increases in T-type channel surface expression would be reflected by increases in maximum T-type current in which all channels are fully deinactivated and then fully activated. To measure maximal Ca^{2+} current, neurons were deinactivated by hyperpolarizing the membrane 75 mV from the holding potential for 1300 ms, then eliciting peak current by stepping back to the holding potential. Before recording currents, the holding potential for each cell was adjusted to a level that would produce the maximum current for the given protocol, therefore maximum current and current density averages for all cohorts are based on the largest possible elicited current for each cell. The average holding potentials for each group are given in Table 2. During the period of SE, there was no significant difference in the maximum current amplitude, capacitance or current density between control and pilo-SE mice (Fig. 3). However, at 10 d after treatment the average maximum current amplitude measured from mice that experienced SE ($n = 8$) was significantly increased by 39.9% com-

Table 2. Summary of electrophysiology data

	4 h saline	4 h pilo	10 d saline	10 d pilo	31 d saline	31 d pilo
Holding potential (mV)	−70.9 ± 1.4 (7)	−69.3 ± 0.5 (9)	−68.1 ± 0.9 (8)	−71.8 ± 1.4 (8)	−68.7 ± 0.8 (12)	−66.9 ± 0.7 (15)
Resistance (MΩ)	150.4 ± 21.7 (7)	188.4 ± 24.1 (9)	173.2 ± 20.3 (8)	141.2 ± 17.0 (8)	247.2 ± 22.6 (12)	216.0 ± 12.9 (15)
Capacitance (pF)	71.2 ± 5.6 (7)	74.7 ± 4.7 (9)	71.3 ± 3.7 (8)	109.7 ± 13.0 (8)**	68.5 ± 3.8 (12)	67.6 ± 3.6 (15)
Maximum current (pA)	672.7 ± 90.5 (7)	682.0 ± 73.5 (9)	659.5 ± 83.4 (8)	939.2 ± 85.5 (8)*	591.0 ± 36.5 (12)	905.3 ± 48.8 (15)***
Current density (pA/pF)	9.4 ± 0.9 (7)	9.3 ± 1.0 (9)	9.4 ± 1.3 (8)	9.3 ± 1.4 (8)	9.6 ± 0.6 (12)	13.7 ± 1.0 (15)***
Activation V_{50} (mV)	−77.4 ± 1.8 (6)	−76.2 ± 1.9 (6)	−74.9 ± 1.4 (8)	−81.7 ± 1.9 (6)*	−75.8 ± 1.8 (8)	−74.8 ± 1.1 (8)
Inactivation V_{50} (mV)	−88.3 ± 1.8 (7)	−85.3 ± 1.2 (9)	−85.8 ± 1.2 (8)	−90.8 ± 1.5 (8)*	−86.7 ± 1.4 (12)	−80.4 ± 0.6 (15)***
Decay constant (ms)	12.4 ± 0.8 (7)	12.7 ± 0.5 (9)	12.5 ± 1.2 (8)	16.6 ± 0.8 (8)*	12.2 ± 0.5 (12)	13.9 ± 0.4 (15)*
Maximum charge (pC)	12.4 ± 1.1 (7)	12.6 ± 1.1 (9)	12.8 ± 2.0 (8)	21.8 ± 1.5 (8)**	11.6 ± 1.0 (12)	15.8 ± 0.9 (15)**
Charge density (pC/pF)	0.22 ± 0.02 (7)	0.21 ± 0.03 (9)	0.18 ± 0.01 (8)	0.20 ± 0.01 (8)	0.19 ± 0.02 (12)	0.25 ± 0.01(15)*

*$p < 0.05$, **$p < 0.01$, ***$p < 0.001$; unpaired *t* test. *n* values are given in parentheses.

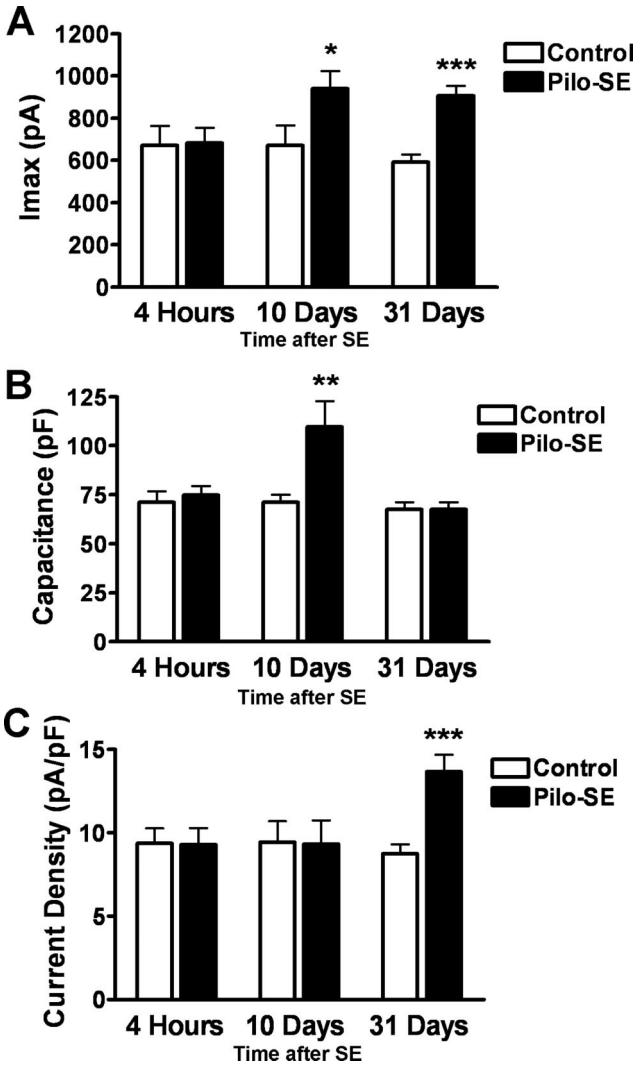

Figure 3. SE alters maximum Ca^{2+} currents and membrane capacitance 10 and 31 d after onset. ***A***, SE does not affect maximally elicited Ca^{2+} currents 4 h after onset (controls, $n = 7$; pilo-SE, $n = 9$), whereas maximally elicited Ca^{2+} currents were increased by 39.9% at 10 d after SE (controls, $n = 8$; pilo-SE, $n = 8$; *$p < 0.05$, unpaired *t* test) and 53.2% at 31 d after SE (controls, $n = 12$; pilo-SE, $n = 15$; ***$p < 0.001$, unpaired *t* test). ***B***, At 10 d after SE, there is a significant increase in membrane capacitance compared with controls ($n = 8$; **$p < 0.01$, unpaired *t* test), but no difference in capacitance was observed between control and pilo-SE cohorts at the 4 h and 31 d time points. ***C***, When the maximum elicited current was normalized to membrane capacitance, there was no difference in overall current density at 10 d between control and pilo-SE animals, the time point corresponding to a latent period before seizure onset. However at 31 d, the current density was significantly increased by 57.5% in the pilo-SE group ($n = 15$) when compared with controls ($n = 12$; ***$p < 0.001$, unpaired *t* test).

pared with control mice ($n = 8$) (Fig. 3*A*, $p < 0.05$, unpaired *t* test), which is consistent with the results shown in Figure 2 showing an increase in $Ca_V3.2$ and $Ca_V3.3$ gene expression. Capacitance measures shown in Figure 3*B* demonstrate that the pilo-SE group also displayed a 53.9% increase in membrane capacitance ($p < 0.01$, unpaired *t* test), which resulted in no change in current density once currents were normalized to membrane capacitance (Fig. 3*C*), indicating that there is no net change in overall T-type current per neuron.

This increase in thalamic neuronal membrane capacitance in the pilo-SE group during the latent period could be attributed to pathophysiological changes in the thalamus that are related to epileptogenesis, but may be more subtle than the increased fiber sprouting that has been shown to occur in the hippocampus during this period (Dalby and Mody, 2001). Interestingly, Chemin et al. (2002) demonstrated a role for $Ca_V3.2$ currents in inducing neuritogenesis and the expression of high voltage-activated calcium channels in an early-differentiating neuronal cell line, suggesting that the increase in capacitance seen 10 d after SE may be attributable to a $Ca_V3.2$-elicited increase in membrane area.

During the chronic SRS period, we also measured a significant increase in current amplitude from pilo-SE mice compared with controls (53.2%) (Fig. 3*A*; controls, $n = 12$; pilo-SE, $n = 15$; $p < 0.001$, unpaired *t* test). No changes in membrane capacitance were observed (Fig. 3*B*), therefore when maximal Ca^{2+} currents were normalized to membrane capacitance, a 57.5% increase in current density was observed for mice 31 d after SE (Fig. 3*C*; controls, $n = 12$; pilo-SE, $n = 15$; $p < 0.001$, unpaired *t* test). This observation suggests that any membrane changes measured at 10 d after SE have dissipated, whereas the enhancement of the T-type current remains.

Steady-state gating properties

Alterations in T-type channel amplitude may be related to transcriptional mechanisms, but for a complete determination of the significance of such changes it is necessary to also examine channel gating properties, which are known to be affected by numerous factors (Mu et al., 2003; Perez-Reyes, 2003; Chemin et al., 2006). The average voltage-dependent activation and inactivation of the T-type Ca^{2+} current is illustrated in Figure 4. T-type current was inactivated by a series of depolarizing command potentials, progressing at 3 mV increments, starting at a 60 mV hyperpolarizing prepulse potential and stepping to the holding potential (Fig. 4*E*). Steady-state activation was determined by hyperpolarizing 40 mV from the holding potential then progressing in 2 mV depolarizing steps until the channels were activated (Fig. 4*F*). Peak current for each step was normalized to the maximally elicited current (I/I_{max}) and was plotted against its respective prepulse potential. The inactivation data were fitted with a

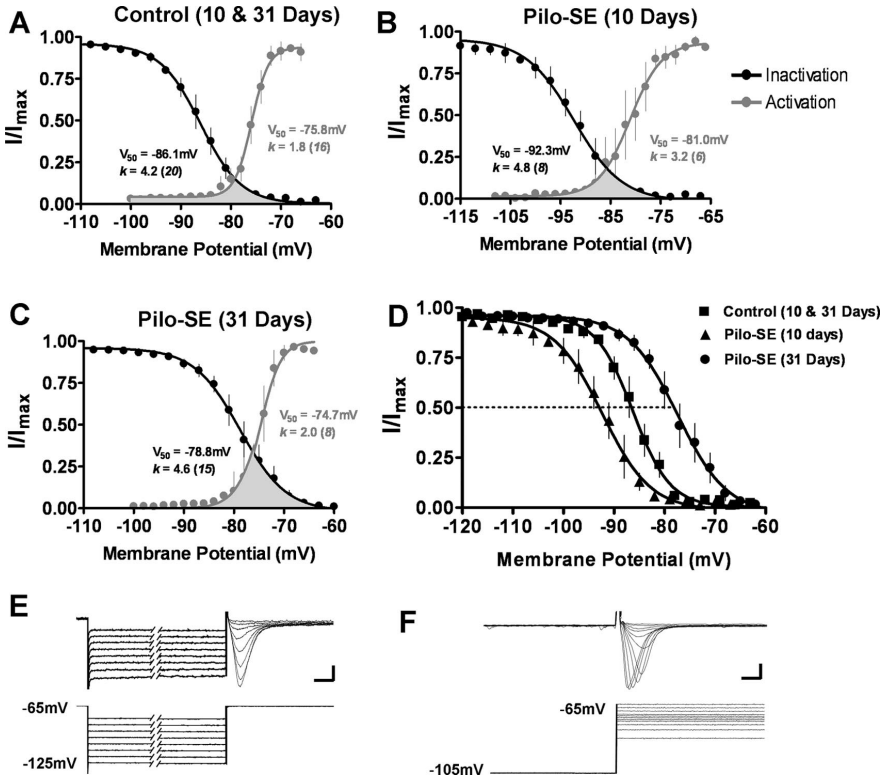

Figure 4. ***A–F***, T-type channel inactivation properties are altered 10 and 31 d post SE Steady-state activation and inactivation curves for 10 and 31 d control (***A***), 10 d pilo-SE (***B***), and 31 d pilo-SE (***C***). The V_{50}, slope (k) and n values for the fitted curves are shown on the graphs. The window current is represented by the shaded region beneath the activation and inactivation curves. ***D***, Graph comparing inactivation data from 10 and 31 d post-SE. There were no differences between control data from mice at 10 and 31 d, therefore these data were combined (squares, $n = 20$) for comparison of pilo-SE cohorts. A hyperpolarizing shift was seen 10 d after SE (circles, $n = 8$; $p < 0.05$, unpaired t test), and a depolarizing shift 31 d after SE (triangles, $n = 15$; $p < 0.001$, unpaired t test). ***E***, ***F***, Representative voltage clamp traces demonstrating the graded, voltage-dependent inactivation (***E***) and activation (***F***) of T-type currents are shown, indicating a well clamped neuron. Calibration: 25 ms, 250 pA.

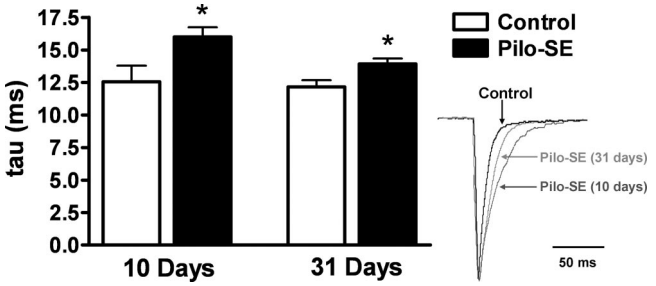

Figure 5. SE produces slower T-type channel decay kinetics 10 and 31 d after onset. Voltage-clamp traces were fit with a standard exponential function to calculate the decay constant (tau) of the elicited currents. At both 10 ($n = 8$) and 31 d ($n = 15$) post-SE, T-type currents from pilo-SE mice displayed significantly slower decay constants compared with controls (10 d, $n = 8$; 31 d, $n = 12$; $^*p < 0.05$, unpaired t test) consistent with the upregulation of T-channel isoforms possessing slower inactivation kinetics. Inset: Representative voltage clamp traces demonstrating slower T-channel decay kinetics for a midline thalamic relay neurons from a 10 d post-SE animal (dark gray) and 31 d post-SE animal (light gray) compared with a cell from a control animal (black). Traces have been normalized and superimposed so that all current peaks overlap. Calibration: 50 ms.

single-sided Boltzmann function and the activation data were fitted with a double-sided Boltzmann equation, and V_{50} values were obtained (Table 2). The V_{50} represents the membrane potential at which the half-maximal current is elicited. Shifts in the V_{50} inactivation values to more depolarized or hyperpolarized potentials are interpreted as either increased or decreased channel availability respectively, contributing to a "window current" that represents a set of membrane potentials in which a fraction of channels are not fully inactivated and remain available to conduct current (Hughes et al., 1999; Crunelli et al., 2005). This window current is represented by the shaded regions underneath the activation and inactivation curves in Figure 4*A–C*. There were no differences between 10 and 31 d control cohorts, therefore the data from those groups were pooled (Fig. 4*A*) for comparison to pilo-SE groups. No significant changes in the V_{50} were seen between control and pilo-SE mice 4 h postinjection (Table 2). However at 10 d postinjection (Fig. 4*B*), the steady-state activation and inactivation curves for thalamic neurons recorded from pilo-SE mice were significantly shifted 6.8 mV and 5 mV respectively, to a more hyperpolarized membrane potential compared with control mice, indicating a decrease in available T-type channels around resting membrane potentials, because a greater membrane hyperpolarization is required to produce similar amounts of T-type current. At 31 d post-SE (Fig. 4*C*), the inactivation curve for midline thalamic neurons was significantly shifted 6.3 mV to a more depolarized range compared with controls, indicating an increase in the amount of available T-type channel current around resting membrane potentials. This results from a larger fraction of T-channels being deinactivated by smaller membrane hyperpolarizations, which in turn could promote greater excitability during the period of SRS.

Inactivation kinetics

Electrophysiological recordings from cell lines engineered to express the three different T-channel isoforms have revealed differences in their biophysical properties, with $Ca_V3.2$ and $Ca_V3.3$ exhibiting slower inactivation kinetics than $Ca_V3.1$ (Chemin et al., 2002). It would then be expected that the upregulation of channels that inactivate more slowly would produce slower decay kinetics in the whole-cell Ca^{2+} current. Therefore, we fitted all recorded currents with a standard exponential function to calculate an average decay constant (tau) for each cell. Figure 5 shows that at 10 and 31 d post-SE, midline thalamic T-currents exhibit slower inactivation kinetics as demonstrated by significantly larger taus (Table 2; 10 d pilo-SE, 16.6 ± 0.8 ms, $n = 8$; 31 d pilo-SE, 13.9 ± 0.4 ms, $n = 15$; $p < 0.05$, unpaired t test). An example of this slower rate of decay is shown in Figure 5. No differences in decay were observed between the 4 h pilo-SE and control groups (Table 2).

The functional implication of a slower current decay is that a greater net charge is conducted through the T-type channels. These data are shown in Table 2 and demonstrate significant increases in maximum charge for both 10 and 31 d pilo-SE cohorts, however once normalized to capacitance, charge density is only significantly increased in the 31 d pilo-SE group (Table 2; $^*p < 0.05$, $^{**}p < 0.01$; unpaired t test).

Ascorbate and Ni^{2+} reduce SE-altered native T-type current

Recently it has been shown by Nelson et al. (2007) that ascorbate can specifically inhibit $Ca_V3.2$ channels, without affecting $Ca_V3.1$ or $Ca_V3.3$. $Ca_V3.2$ is also much more sensitive than the other T-type isoforms to blockade by Ni^{2+} (Lee et al., 1999). We therefore tested the effects of ascorbate and Ni^{2+} on midline thalamic neurons from 31 d post-SE and on neurons from control cohorts to determine whether $Ca_V3.2$ channels play a role in the SE-induced changes we observed in native T-type channel properties.

Figure 6*A* shows the time course and raw traces of the effect of 1 mM ascorbate on midline thalamic T-type currents in a mouse 31 d after SE. Ascorbate treatment resulted in an average reduction of the native T-type current to 87.6 ± 2.9% of baseline in pilo-SE animals ($n = 8$, $p < 0.05$, paired *t* test), but had no effect on T-type currents recorded from control animals at 31 d postsaline treatment (Fig. 6*B*; 100.5 ± 1.7% of baseline, $n = 3$). Figure 6*C* shows the effect of 1 mM ascorbate on burst firing in midline thalamic neurons from both a control (top) and pilo-SE mouse (bottom). Bursts were elicited in 31 d pilo-SE cells by injection of a 50 pA hyperpolarizing current for 500 ms before stepping to the holding potential. Bursts in control cells were elicited by 100 pA hyperpolarizing current for 500 ms. Ascorbate reduced the number of action potentials in low-threshold Ca^{2+} spike bursts only in the 31 d pilo-SE cells from 4.0 ± 0.4 to 2.2 ± 1.6, followed by a partial recovery during washout, 3.3 ± 0.4 ($n = 4$). To further verify the involvement of a $Ca_V3.2$-specific current, we tested the effects of 50 and 100 μM Ni^{2+} on 31 d control and pilo-SE cells (Fig. 6*D*). We found a similar partial inhibition of the native T-type current, with 50 μM Ni^{2+} reducing the current to 87.1 ± 2.1% of the baseline ($n = 8$; $p < 0.05$, paired *t* test) and 100 μM Ni^{2+} reducing the current to 79.7 ± 4.0% of the baseline ($n = 3$; $p < 0.05$, paired *t* test), without effecting the native T-type current in control mice (97.1 ± 4.2% of the baseline, $n = 5$).

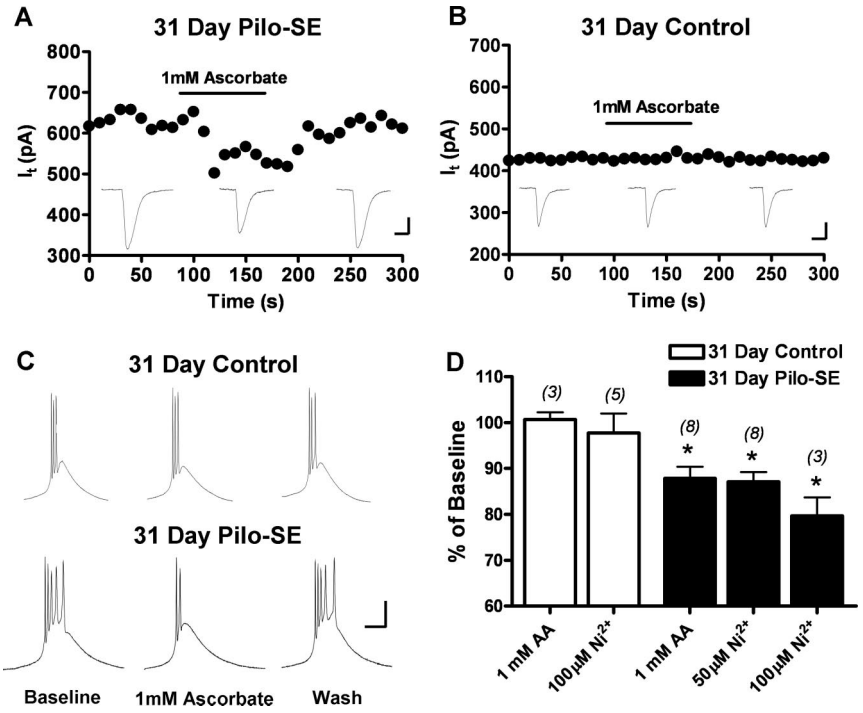

Figure 6. Ascorbate and Ni^{2+} partially inhibit native T-type Ca^{2+} currents from midline thalamic neurons 31 d after SE. ***A***, Time course showing the rapid onset of a partial inhibition of the native T-type current in midline thalamic neuron from a mouse 31 d after SE after introduction of 1 mM ascorbate into the bath solution. Representative traces from baseline, treatment and washout periods, respectively, are shown on the graph. Calibration: 200 pA, 25 ms. ***B***, Time course showing no effect of ascorbate on midline thalamic T-current from 31 d control animal. Representative traces from baseline, treatment and washout periods, respectively, are shown on the graph. Calibration: 200 pA, 25 ms. ***C***, Representative current-clamp traces from a 31 d control (top) and 31 d pilo-SE (bottom) mouse showing that 1 mM ascorbate reduces the amount of action potentials per burst elicited by the low-threshold Ca^{2+} spike only in mice that experienced SE. Calibration: 25 mV, 50 ms. ***D***, Bar graph showing the average partial inhibition of the native T-type current with 1 mM ascorbate (AA), 50 μM Ni^{2+}, and 100 μM Ni^{2+} as represented by the mean percent of the baseline while the drug was in the bath solution. The numbers for each group are given above the bars (*$p < 0.05$, paired *t* test).

SE produces changes in low-threshold Ca^{2+} bursts

Figure 7 shows the responses of 31 d control and pilo-SE midline thalamic relay neurons to varying amounts of hyperpolarizing currents preceding depolarizing steps to different membrane potentials. As demonstrated by the surface plots generated from data collected in current-clamp mode (Fig. 7*A*,*B*), bursts were elicited at 68.9% of the points with an average of 4.5 ± 0.1 spikes per burst ($n = 143$, 4 cells) for 31 d control mice and 75.0% of the points with an average of 6.7 ± 0.1 spikes per burst ($n = 107$, 7 cells; $p < 0.0001$, unpaired *t* test) for 31 d pilo-SE. This increase in excitability is most notable around resting conditions (−65 mV) at which a burst can be generated by a 50 pA hyperpolarizing current pulse in a cell from a 31 d pilo-SE animal (Fig. 7*B*, *t*race 3), but not from a cell recorded from a control mouse (Fig. 7*A*, *t*race 1). We also observed that the majority of total bursts elicited from 31 d pilo-SE neurons (72.9%) produced 7 or more action potentials per burst, compared with only 6.3% for 31 d control cells.

We then created a computational model based on a modified version of the integrate-and-fire-or-burst (IFB) model constructed by Smith et al. (2000), to model the alterations we observed in T-type channel currents and reproduce the changes in low-threshold Ca^{2+} bursts cause by SE (Fig. 8). Our model, incorporating empirical data gathered during voltage-clamp recordings, allows for testing neuronal burst responses at a more expansive parameter space, providing a comprehensive, descriptive data set that is less feasible with empirical measures. The model produced similar surface plots for both 31 d control midline thalamic neurons (66.9%, 3.1 average spikes per burst) (Fig. 8*A*) and 31 d post-SE cells (74.9%, 7.4 spikes per burst) (Fig. 8*C*) to those constructed from current-clamp recordings. A surface plot generated by the model from 10 d pilo-SE data (Fig. 8*B*) produced bursts at 43.3% of the tested points, with an average of 3.7 spikes per burst, indicating that even though we observed an increase in T-type channel expression and maximum current at this time point after SE, steady-state properties and current density play a larger role in determining thalamic excitability. Representative traces generated by the model from control data (1,2), 10 d pilo-SE data (3,4), and 31 d pilo-SE data (5,6) are shown to the right of the model-derived surface plots (Fig. 8*A–C*). We also derived a burst index from the surface plots generated by the model as a measure to gauge neuronal excitability in all cohorts

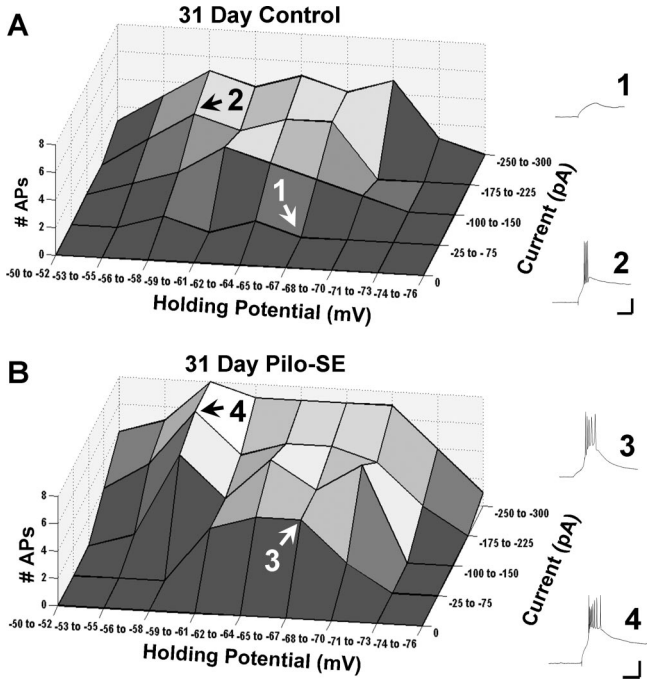

Figure 7. SE-elicited alterations in T-type currents produce changes in burst responses that are consistent with observed differences in excitability. Surface plots demonstrating the burst profile for midline thalamic neurons from 31 d control mice (***A***, $n = 4$), and 31 d pilo-SE mice (***B***, $n = 7$). The plots show the number of action potentials per burst (*z*-axis) resulting from changes in the holding potential (*x*-axis) and the amount of hyperpolarizing current before stepping to the holding potential (*y*-axis). These plots show elicited bursts at 68.9% of the points with an average of 4.5 ± 0.1 spikes per burst ($n = 143$) for 31 d control mice and 75.0% of the points with an average of 6.7 ± 0.1 spikes per burst ($n = 107$; $p < 0.0001$, unpaired *t* test) for 31 d pilo-SE. Representative traces illustrating burst discharges (1–4) are shown to the right of the plots. Traces 1 and 3 were at a holding potential of −65 mV with a −50 pA injected current. Traces 2 and 4 were at a holding potential of −58 mV with a −200 pA injected current. Calibration: 25 mV, 50 ms.

(Fig. 8*D*). This burst index demonstrates relatively equivalent excitability across all groups except the 31 d pilo-SE cohort, which exhibits a dramatically larger burst index, indicating a hyperexcitable population of thalamic neurons that coincides with the chronic SRS period of the pilocarpine SE model.

Discussion

Our study describes an acquired channelopathy involving thalamic T-type Ca^{2+} channels in a mouse model of acquired epilepsy. We found an increase in $Ca_V3.2$ gene expression in the midline thalamic nuclei during both the chronic phase of SRS and the preceding latent period after SE, as well as a significant increase in $Ca_V3.3$ gene expression during the latent period. We have also shown that these changes are functionally relevant by demonstrating concomitant larger peak currents and longer current decays in both post-SE cohorts, consistent with the upregulation of $Ca_V3.2$ and $Ca_V3.3$, as well as an increase in T-type current density during the period of SRS. We also demonstrated shifts in steady-state properties to more hyperpolarized membrane potentials during the latent phase and more depolarized potentials during the chronic phase, both of which are consistent with the absence or appearance (respectively) of SRS in the pilocarpine model. Additionally, we were able to isolate an ascorbate and Ni^{2+}-sensitive T-type current in a 31 d post-SE cohort that was not present in controls, consistent with the upregulation of $Ca_V3.2$. Finally, through both current-clamp recordings and modeling of voltage-clamp data, we showed that SE-elicited alterations in T-type currents reduced the amount of burst responses seen during the latent period, and promoted a greater tendency to burst during the chronic phase.

Several channelopathies have been associated with epileptogenesis and seizure syndromes, but in animal models most derive from genetic differences in expression of certain ion channels that promote seizure. However, many epilepsies do not possess clearly inherited genetic linkages. Our results add to the literature suggesting that in addition to genetic channelopathies, there may be circumstances under which channelopathies may be acquired, resulting from neural activity occurring during SE (Bernard et al., 2004; Jung et al., 2007; Becker et al., 2008).

Numerous mutations in the $Ca_V3.2$ gene leading to an increase in T-type channel activity have been identified in patients diagnosed with childhood absence epilepsy, as well as other forms of idiopathic generalized epilepsy (Khosravani et al., 2004, 2005; Khosravani and Zamponi, 2006). These types of generalized seizures have been shown to involve synchronized thalamocortical oscillations generated by thalamic T-type currents (Shin, 2006). Bertram et al. (1998) hypothesized that because of strong, widespread excitatory reciprocal connections between midline thalamic and limbic structures (Dolleman-Van der Weel MJ et al., 1997; Bertram and Zhang, 1999), midline thalamic neurons may play an important role in the generation and propagation of ictal events stemming from temporal lobe structures. Specifically, increased RE output through hyperexcitable neurons may amplify hippocampal activity through two means: by enhancing pathophysiological burst activity associated with increased CA1 dendritic T-type currents (Yaari et al., 2007), and by dysregulating the temporoammonic pathway (Ang et al., 2006) through an augmented excitatory drive onto the entorhinal cortex (Fig. 9). Moreover, reciprocal connections between the RE and CA1, which both send collaterals to the thalamic reticular nucleus (TRN), comprise a thalamo-hippocampal loop that is of a similar pattern to the thalamocortical loop between thalamic relay neurons and sensory cortices (Cavdar et al., 2008). The circuit between the TRN and thalamic neurons possesses a strong pacemaker function and has been implicated in the generation of seizures and seizure disorders (Avanzini et al., 2000). A RE-TRN-CA1 loop may amplify ictal activity in the hippocampus, leading to seizure generalization by recruiting additional thalamocortical circuits into synchronized activity. Interestingly, Ferreira et al. (2003) recorded synchronized absence-like spike-wave discharges (SWD) from the thalamus, hippocampus and cortex of adult rats that had experienced pilocarpine-induced SE. These SWD were abolished with ethosuximide, a broad-spectrum T-type channel blocker. The involvement of a limbic-thalamic epileptogenic network in the generalization of seizures has also been demonstrated in imaging studies of human TLE patients showing associated temporal lobe and thalamic activity (Blumenfeld et al., 2004), and increased EEG synchrony between the thalamus and temporal lobe structures during temporal lobe seizures (Guye et al., 2006).

It has previously been shown that the development of seizures in the pilocarpine model is associated with the appearance of spontaneous bursting in hippocampal neurons resulting from an upregulation of dendritic $Ca_V3.2$ currents (Sanabria et al., 2001; Su et al., 2002; Yaari et al., 2007; Becker et al., 2008). Although some have shown increased hippocampal bursting during the SRS period (Sanabria et al., 2001; Su et al., 2002), others have demonstrated transient hippocampal changes in $Ca_V3.2$ expression and neuronal bursting that lead to significant CA1 and CA3 neuronal loss during the later stages (Becker et al., 2008). An

enhancement of neuronal bursting has also been reported in the midline thalamic nuclei in a kindling model of limbic epilepsy (Bertram et al., 2001). Our results further demonstrate a complex sequence of molecular and physiological changes in midline thalamic T-type channels during both the development and appearance of SRS that account for the early period of decreased tendency to participate in bursting, as well as the later SRS period that is characterized by the presence of such bursts. Our findings of enhanced midline thalamic bursting during the chronic SRS stage support those of Bertram et al. (2001) and raise the question whether the SE-induced pathophysiological alterations in wild-type mice, but not $Ca_V3.2$ KO mice, observed by Becker et al. (2008) are solely the result of intrinsic changes mediated by hippocampal T-type channels, or may also be the result of abnormal input from midline thalamus.

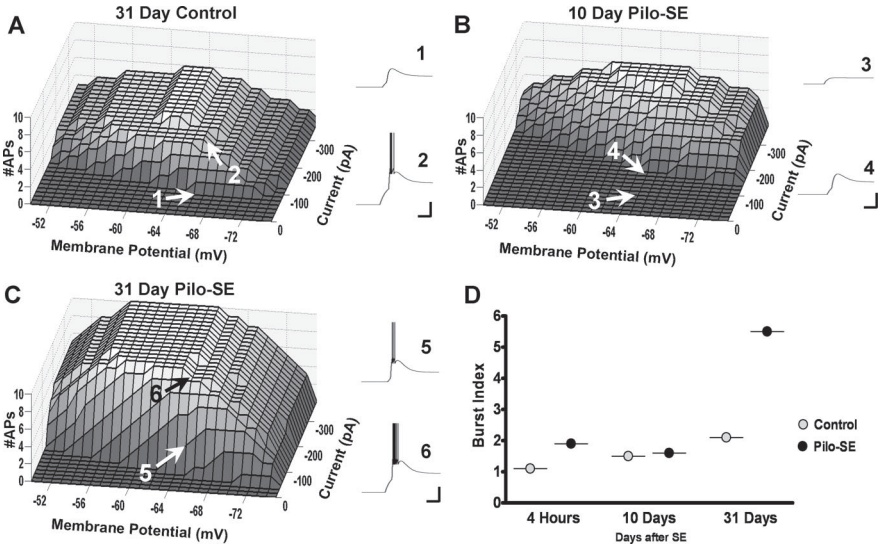

Figure 8. Modeled burst responses predict changes in thalamic excitability consistent with the absence and appearance of SRS. ***A***, A surface plot generated by the model for 31 d control cohorts produced 66.9% bursts, with an average of 3.1 spikes per burst. The model generated a similar surface plot for 10 d control cohorts (data not shown). Modeled traces (1,2) for representative points on the plot are shown to the right; holding potential −65 mV, injected current −75 pA and −150 pA. ***B***, Surface plot generated by the model for 10 d pilo-SE cohorts produced 43.3% bursts, with an average of 3.7 spikes per burst. Modeled traces (3,4) for representative points on the plot are shown to the right; same parameters as in ***A***. ***C***, A surface plot generated by the model for 31 d pilo-SE cohorts produced 74.9% bursts, with an average of 7.4 spikes per burst. The 31 d pilo-SE model predicts greater overall excitability at a wider range of voltages than either the 10 d model or the model derived from 31 d controls. Modeled traces (5,6) for representative points on the plot are shown to the right; same parameters as in ***A*** and ***B***. ***D***, A burst index was calculated from the modeled surface plots for each group by multiplying the percentage of generated bursts by the average number of action potentials per burst. A large increase in the burst index is seen in the data modeled from 31 d pilo-SE mice.

This last point is particularly important because of the distinction between our results and those of Becker et al. (2008) in the time course during which the observed changes are occurring in these two neuronal populations. We have shown that changes in thalamic burst discharges correspond to the absence or appearance of SRS after SE, and that this decreased or increased excitability is due both to an upregulation of $Ca_V3.2$ and alterations in steady-state channel properties. Further investigation is needed to determine whether or not the initial upregulation of $Ca_V3.2$-dependent hippocampal bursts causes $Ca_V3.2$-specific thalamic changes through the reciprocal, excitatory connections between CA1 and RE. Regardless of the mechanism, our results are consistent with an important role of the thalamus in supporting SRS.

Shifts in T-type channel steady-state properties can either increase or decrease the available T-type current around resting membrane potentials (Hughes et al., 1999; Crunelli et al., 2005), therefore changes in steady-state inactivation should correlate to alterations in neuronal bursting. Indeed, depolarizing shifts in T-channel steady-state inactivation have been associated with SWD observed in certain mouse models of absence epilepsy (Zhang et al., 2004). Both our current-clamp recordings and computational model reflecting observed shifts in steady-state properties verified that the hyperpolarizing shift during the silent phase was consistent with a reduced propensity to burst, whereas a depolarizing shift during the period corresponding to the appearance of SRS enhanced hyperexcitability and bursting. Alterations in burst responses therefore appear to be determined by a complex sequence of altered $Ca_V3.2$ gene expression and T-type current density, in tandem with changes in the voltage-dependent properties.

Whereas the slower decay kinetics that we saw at 10 and 31 d post-SE are best explained by upregulation of $Ca_V3.2$ and $Ca_V3.3$, shifts in the steady-state inactivation properties are more likely to arise through regulation of channel function. Newly expressed $Ca_V3.2$ channels represent a likely target, because this isoform has been shown to possess multiple means of modulation, with reports of several different endogenous kinases, hormones, divalent metals and reducing agents that can both enhance and inhibit its function (Ferron et al., 2003; Welsby et al., 2003; Joksovic et al., 2006; Kim et al., 2006; Park et al., 2006; Huh et al., 2008; Tao et al., 2008). Both the hyperpolarizing shift at 10 d and the depolarizing shift at 31 d could be caused by modulation of upregulated $Ca_V3.2$ channels by one or multiple factors.

One endogenous regulator of $Ca_V3.2$ is Zn^{2+}, and Zn^{2+} levels are significantly reduced in the thalamus, specifically the RE, of chronically epileptic rats after pilocarpine treatment (Hamani et al., 2005). Traboulsie et al. (2007) demonstrated that $Ca_V3.2$ is significantly more sensitive to inhibition by Zn^{2+} than $Ca_V3.1$ and $Ca_V3.3$, and that this inhibition is associated with a hyperpolarizing shift in the steady-state inactivation curve of all three isoforms. These results support the idea that a portion of the increased thalamic T-channel function seen during the chronic SRS period could be the result of reduced endogenous regulation of $Ca_V3.2$ by Zn^{2+}. However, additional studies investigating alterations of the second messenger pathways known to modulate T-type channels are needed to fully elucidate the mechanisms responsible for the observed changes in channel expression and function.

Our results reveal a sequence of increased expression and altered gating properties of thalamic T-type channels that coincides with the essential physiological phases of epileptogenesis in the pilocarpine model. Our study is consistent with previous literature, but illustrates several distinctive changes involving thalamic T-type channel physiology that underlie the amplification and propagation of limbic ictal activity leading to generalized seizures. These findings further open the door to investigations involving the modulation of intrinsic neuronal excitability with

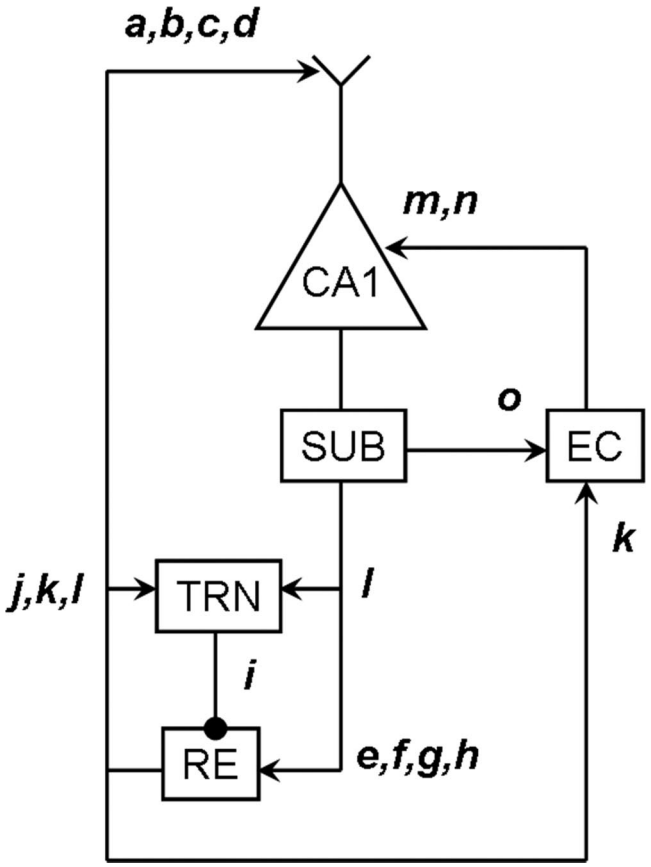

Figure 9. Schematic representation of the RE-TRN-CA1 loop. Diagram showing the reciprocal excitatory connections (arrows) between RE and CA1 along with emitted collaterals into the TRN. The inhibitory connection (circle) between the TRN and RE is also shown. In addition, the RE sends excitatory projections to the entorhinal cortex (EC), which is part of its own excitatory loop involving CA1 and the subiculum (SUB). References: a, Wouterlood et al. (1990); b, Dolleman-Van der Weel and Witter (1996); c, Dolleman-Van der Weel et al. (1997); d, Bertram and Zhang (1999); e, Herkenham (1978), f, Aggleton et al. (1986); g, Witter et al. (1990); h, Dolleman-Van der Weel et al. (1993); i, McKenna and Vertes (2004); j, Cornwall et al. (1990); k, Vertes et al. (2006); l, Cavdar et al. (2008); m, Doller and Weight (1982); n, Witter et al. (1988); o, Tamamaki and Nojyo (1995).

agents such as ascorbate by specifically targeting upregulated $Ca_V3.2$ channels. Although there is evidence that ascorbate is neuroprotective against chemically induced seizures during epileptogenesis in animal models (Ayyildiz et al., 2007; Xavier et al., 2007; Santos et al., 2008), future studies investigating the behavioral effects of ascorbate during the chronic phase of SRS are needed to determine the role ascorbate could play in a potential treatment for the one-third of TLE patients resistant to current pharmacotherapies.

References

Aggleton JP, Desimone R, Mishkin M (1986) The origin, course, and termination of the hippocampothalamic projections in the macaque. J Comp Neurol 243:409–421.

Alexander GM, Carden WB, Mu J, Kurukulasuriya NC, McCool BA, Nordskog BK, Friedman DP, Daunais JB, Grant KA, Godwin DW (2006) The native T-type calcium current in relay neurons of the primate thalamus. Neuroscience 141:453–461.

Ang CW, Carlson GC, Coulter DA (2006) Massive and specific dysregulation of direct cortical input to the hippocampus in temporal lobe epilepsy. J Neurosci 26:11850–11856.

Avanzini G, Panzica F, de Curtis M (2000) The role of the thalamus in vigilance and epileptogenic mechanisms. Clin Neurophysiol 111 [Suppl 2]:S19–S26.

Ayyildiz M, Coskun S, Yildirim M, Agar E (2007) The effects of ascorbic acid on penicillin-induced epileptiform activity in rats. Epilepsia 48:1388–1395.

Barber RD, Harmer DW, Coleman RA, Clark BJ (2005) GAPDH as a housekeeping gene: analysis of GAPDH mRNA expression in a panel of 72 human tissues. Physiol Genomics 21:389–395.

Becker AJ, Pitsch J, Sochivko D, Opitz T, Staniek M, Chen CC, Campbell KP, Schoch S, Yaari Y, Beck H (2008) Transcriptional upregulation of Cav3.2 mediates epileptogenesis in the pilocarpine model of epilepsy. J Neurosci 28:13341–13353.

Bernard C, Anderson A, Becker A, Poolos NP, Beck H, Johnston D (2004) Acquired dendritic channelopathy in temporal lobe epilepsy. Science 305:532–535.

Bertram EH, Zhang DX (1999) Thalamic excitation of hippocampal CA1 neurons: a comparison with the effects of CA3 stimulation. Neuroscience 92:15–26.

Bertram EH, Zhang DX, Mangan P, Fountain N, Rempe D (1998) Functional anatomy of limbic epilepsy: a proposal for central synchronization of a diffusely hyperexcitable network. Epilepsy Res 32:194–205.

Bertram EH, Mangan PS, Zhang D, Scott CA, Williamson JM (2001) The midline thalamus: alterations and a potential role in limbic epilepsy. Epilepsia 42:967–978.

Bertram EH, Zhang D, Williamson JM (2008) Multiple roles of midline dorsal thalamic nuclei in induction and spread of limbic seizures. Epilepsia 49:256–268.

Blumenfeld H, McNally KA, Vanderhill SD, Paige AL, Chung R, Davis K, Norden AD, Stokking R, Studholme C, Novotny EJ Jr, Zubal IG, Spencer SS (2004) Positive and negative network correlations in temporal lobe epilepsy. Cereb Cortex 14:892–902.

Carden WB, Alexander GM, Friedman DP, Daunais JB, Grant KA, Mu J, Godwin DW (2006) Chronic ethanol drinking reduces native T-type calcium current in the thalamus of nonhuman primates. Brain Res 1089:92–100.

Cavdar S, Onat FY, Cakmak YO, Yananli HR, Gülçebi M, Aker R (2008) The pathways connecting the hippocampal formation, the thalamic reuniens nucleus and the thalamic reticular nucleus in the rat. J Anat 212:249–256.

Chemin J, Monteil A, Perez-Reyes E, Bourinet E, Nargeot J, Lory P (2002) Specific contribution of human T-type calcium channel isotypes (alpha(1G), alpha(1H) and alpha(1I)) to neuronal excitability. J Physiol 540:3–14.

Chemin J, Traboulsie A, Lory P (2006) Molecular pathways underlying the modulation of T-type calcium channels by neurotransmitters and hormones. Cell Calcium 40:121–134.

Chen Y, Lu J, Pan H, Zhang Y, Wu H, Xu K, Liu X, Jiang Y, Bao X, Yao Z, Ding K, Lo WH, Qiang B, Chan P, Shen Y, Wu X (2003) Association between genetic variation of CACNA1H and childhood absence epilepsy. Ann Neurol 54:239–243.

Cornwall J, Cooper JD, Phillipson OT (1990) Afferent and efferent connections of the laterodorsal tegmental nucleus in the rat. Brain Res Bull 25:271–284.

Coulter DA (2001) Epilepsy-associated plasticity in gamma-aminobutyric acid receptor expression, function, and inhibitory synaptic properties. Int Rev Neurobiol 45:237–252.

Coulter DA, Huguenard JR, Prince DA (1989) Specific petit mal anticonvulsants reduce calcium currents in thalamic neurons. Neurosci Lett 98:74–78.

Crunelli V, Lightowler S, Pollard CE (1989) A T-type Ca2+ current underlies low-threshold Ca2+ potentials in cells of the cat and rat lateral geniculate nucleus. J Physiol 413:543–561.

Crunelli V, Tóth TI, Cope DW, Blethyn K, Hughes SW (2005) The 'window' T-type calcium current in brain dynamics of different behavioural states. J Physiol 562:121–129.

Dalby NO, Mody I (2001) The process of epileptogenesis: a pathophysiological approach. Curr Opin Neurol 14:187–192.

Dheda K, Huggett JF, Bustin SA, Johnson MA, Rook G, Zumla A (2004) Validation of housekeeping genes for normalizing RNA expression in real-time PCR. Biotechniques 37:112–114, 116, 118–119.

Dolleman-Van der Weel MJ, Ang W, Witter MP (1993) Afferent connections of the nucleus reuniens thalami: a neuroanatomical tracing study in the rat. Eur J Neurosci [Suppl] 6:247.

Dolleman-Van Der Weel MJ, Witter MP (1996) Projections from the nu-

cleus reuniens thalami to the entorhinal cortex, hippocampal field CA1, and the subiculum in the rat arise from different populations of neurons. J Comp Neurol 364:637–650.

Dolleman-Van der Weel MJ, Lopes da Silva FH, Witter MP (1997) Nucleus reuniens thalami modulates activity in hippocampal field CA1 through excitatory and inhibitory mechanisms. J Neurosci 17:5640–5650.

Doller HJ, Weight FF (1982) Perforant pathway activation of hippocampal CA1 stratum pyramidale neurons: electrophysiological evidence for a direct pathway. Brain Res 237:1–13.

Ferreira BL, Valle AC, Cavalheiro EA, Timo-Iaria C (2003) Absence-like seizures in adult rats following pilocarpine-induced status epilepticus early in life. Braz J Med Biol Res 36:1685–1694.

Ferron L, Capuano V, Ruchon Y, Deroubaix E, Coulombe A, Renaud JF (2003) Angiotensin II signaling pathways mediate expression of cardiac T-type calcium channels. Circ Res 93:1241–1248.

Guye M, Régis J, Tamura M, Wendling F, McGonigal A, Chauvel P, Bartolomei F (2006) The role of corticothalamic coupling in human temporal lobe epilepsy. Brain 129:1917–1928.

Hamani C, Paulo I, Mello LE (2005) Neo-Timm staining in the thalamus of chronically epileptic rats. Braz J Med Biol Res 38:1677–1682.

Herkenham M (1978) The connections of the nucleus reuniens thalami: evidence for a direct thalamo-hippocampal pathway in the rat. J Comp Neurol 177:589–610.

Hughes SW, Cope DW, Tóth TI, Williams SR, Crunelli V (1999) All thalamocortical neurones possess a T-type Ca2+ 'window' current that enables the expression of bistability-mediated activities. J Physiol 517:805–815.

Huh SU, Kang HW, Park JY, Lee JH (2008) Regulation of CA. (v) 3.2 Ca2+ channel activity by protein tyrosine phosphorylation. J Microbiol Biotechnol 18:365–368.

Jahnsen H, Llinás R (1984) Voltage-dependent burst-to-tonic switching of thalamic cell activity: an in vitro study. Arch Ital Biol 122:73–82.

Johnson MR, Wang K, Smith JB, Heslin MJ, Diasio RB (2000) Quantitation of dihydropyrimidine dehydrogenase expression by real-time reverse transcription polymerase chain reaction. Anal Biochem 278:175–184.

Joksovic PM, Nelson MT, Jevtovic-Todorovic V, Patel MK, Perez-Reyes E, Campbell KP, Chen CC, Todorovic SM (2006) CaV3.2 is the major molecular substrate for redox regulation of T-type Ca2+ channels in the rat and mouse thalamus. J Physiol 574:415–430.

Jung S, Jones TD, Lugo JN Jr, Sheerin AH, Miller JW, D'Ambrosio R, Anderson AE, Poolos NP (2007) Progressive dendritic HCN channelopathy during epileptogenesis in the rat pilocarpine model of epilepsy. J Neurosci 27:13012–13021.

Khosravani H, Zamponi GW (2006) Voltage-gated calcium channels and idiopathic generalized epilepsies. Physiol Rev 86:941–966.

Khosravani H, Altier C, Simms B, Hamming KS, Snutch TP, Mezeyova J, McRory JE, Zamponi GW (2004) Gating effects of mutations in the Cav3.2 T-type calcium channel associated with childhood absence epilepsy. J Biol Chem 279:9681–9684.

Khosravani H, Bladen C, Parker DB, Snutch TP, McRory JE, Zamponi GW (2005) Effects of Cav3.2 channel mutations linked to idiopathic generalized epilepsy. Ann Neurol 57:745–749.

Kim JA, Park JY, Kang HW, Huh SU, Jeong SW, Lee JH (2006) Augmentation of Cav3.2 T-type calcium channel activity by cAMP-dependent protein kinase A. J Pharmacol Exp Ther 318:230–237.

Lee JH, Gomora JC, Cribbs LL, Perez-Reyes E (1999) Nickel block of three cloned T-type calcium channels: low concentrations selectively block alpha1H. Biophys J 77:3034–3042.

Livak KJ, Schmittgen TD (2001) Analysis of relative gene expression data using real-time quantitative PCR and the 2(−delta delta C(T)) method. Methods 25:402–408.

Lothman EW, Rempe DA, Mangan PS (1995) Changes in excitatory neurotransmission in the CA1 region and dentate gyrus in a chronic model of temporal lobe epilepsy. J Neurophysiol 74:841–848.

McKenna JT, Vertes RP (2004) Afferent projections to nucleus reuniens of the thalamus. J Comp Neurol 480:115–142.

McNamara JO (1994) Cellular and molecular basis of epilepsy. J Neurosci 14:3413–3425.

Meldgaard M, Fenger C, Lambertsen KL, Pedersen MD, Ladeby R, Finsen B (2006) Validation of two reference genes for mRNA level studies of murine disease models in neurobiology. J Neurosci Methods 156:101–110.

Morimoto K, Fahnestock M, Racine RJ (2004) Kindling and status epilepticus models of epilepsy: rewiring the brain. Prog Neurobiol 73:1–60.

Mu J, Carden WB, Kurukulasuriya NC, Alexander GM, Godwin DW (2003) Ethanol influences on native T-type calcium current in thalamic sleep circuitry. J Pharmacol Exp Ther 307:197–204.

Nelson MT, Joksovic PM, Su P, Kang HW, Van Deusen A, Baumgart JP, David LS, Snutch TP, Barrett PQ, Lee JH, Zorumski CF, Perez-Reyes E, Todorovic SM (2007) Molecular mechanisms of subtype-specific inhibition of neuronal T-type calcium channels by ascorbate. J Neurosci 27:12577–12583.

Nordskog BK, Hammarback JA, Godwin DW (2006) Diurnal gene expression patterns of T-type calcium channels and their modulation by ethanol. Neuroscience 141:1365–1373.

Park JY, Kang HW, Moon HJ, Huh SU, Jeong SW, Soldatov NM, Lee JH (2006) Activation of protein kinase C augments T-type Ca2+ channel activity without changing channel surface density. J Physiol 577:513–523.

Peng Z, Huang CS, Stell BM, Mody I, Houser CR (2004) Altered expression of the delta subunit of the GABAA receptor in a mouse model of temporal lobe epilepsy. J Neurosci 24:8629–8639.

Perez-Reyes E (2003) Molecular physiology of low-voltage-activated t-type calcium channels. Physiol Rev 83:117–161.

Sanabria ER, Su H, Yaari Y (2001) Initiation of network bursts by Ca2+-dependent intrinsic bursting in the rat pilocarpine model of temporal lobe epilepsy. J Physiol 532:205–216.

Santos LF, Freitas RL, Xavier SM, Saldanha GB, Freitas RM (2008) Neuroprotective actions of vitamin C related to decreased lipid peroxidation and increased catalase activity in adult rats after pilocarpine-induced seizures. Pharmacol Biochem Behav 89:1–5.

Schmittgen TD, Zakrajsek BA (2000) Effect of experimental treatment on housekeeping gene expression: validation by real-time, quantitative RT-PCR. J Biochem Biophys Methods 46:69–81.

Shibley H, Smith BN (2002) Pilocarpine-induced status epilepticus results in mossy fiber sprouting and spontaneous seizures in C57BL/6 and CD-1 mice. Epilepsy Res 49:109–120.

Shin HS (2006) T-type Ca2+ channels and absence epilepsy. Cell Calcium 40:191–196.

Smith GD, Cox CL, Sherman SM, Rinzel J (2000) Fourier analysis of sinusoidally driven thalamocortical relay neurons and a minimal integrate-and-fire-or-burst model. J Neurophysiol 83:588–610.

Su H, Sochivko D, Becker A, Chen J, Jiang Y, Yaari Y, Beck H (2002) Upregulation of a T-type Ca2+ channel causes a long-lasting modification of neuronal firing mode after status epilepticus. J Neurosci 22:3645–3655.

Sutula T, Cascino G, Cavazos J, Parada I, Ramirez L (1989) Mossy fiber synaptic reorganization in the epileptic human temporal lobe. Ann Neurol 26:321–330.

Talley EM, Cribbs LL, Lee JH, Daud A, Perez-Reyes E, Bayliss DA (1999) Differential distribution of three members of a gene family encoding low voltage-activated (T-type) calcium channels. J Neurosci 19:1895–1911.

Tamamaki N, Nojyo Y (1995) Preservation of topography in the connections between the subiculum, field CA1, and the entorhinal cortex in rats. J Comp Neurol 353:379–390.

Tao J, Hildebrand ME, Liao P, Liang MC, Tan G, Li S, Snutch TP, Soong TW (2008) Activation of corticotropin-releasing factor receptor 1 selectively inhibits CaV3.2 T-type calcium channels. Mol Pharmacol 73:1596–1609.

Traboulsie A, Chemin J, Chevalier M, Quignard JF, Nargeot J, Lory P (2007) Subunit-specific modulation of T-type calcium channels by zinc. J Physiol 578:159–171.

Turski WA, Cavalheiro EA, Schwarz M, Czuczwar SJ, Kleinrok Z, Turski L (1983) Limbic seizures produced by pilocarpine in rats: behavioural, electroencephalographic and neuropathological study. Behav Brain Res 9:315–335.

Vertes RP, Hoover WB, Do Valle AC, Sherman A, Rodriguez JJ (2006) Efferent projections of reuniens and rhomboid nuclei of the thalamus in the rat. J Comp Neurol 499:768–796.

Welsby PJ, Wang H, Wolfe JT, Colbran RJ, Johnson ML, Barrett PQ (2003) A mechanism for the direct regulation of T-type calcium chan-

nels by Ca^{2+}/calmodulin-dependent kinase II. J Neurosci 23:10116–10121.

Winokur RS, Kubal T, Liu D, Davis SF, Smith BN (2004) Recurrent excitation in the dentate gyrus of a murine model of temporal lobe epilepsy. Epilepsy Res 58:93–105.

Witter MP, Griffioen AW, Jorritsma-Byham B, Krijnen JL (1988) Entorhinal projections to the hippocampal CA1 region in the rat: an underestimated pathway. Neurosci Lett 85:193–198.

Witter MP, Ostendorf RH, Groenewegen HJ (1990) Heterogeneity in the dorsal subiculum of the rat. Distinct neuronal zones project to different cortical and subcortical targets. Eur J Neurosci 2:718–725.

Wouterlood FG, Saldana E, Witter MP (1990) Projection from the nucleus reuniens thalami to the hippocampal region: light and electron microscopic tracing study in the rat with the anterograde tracer Phaseolus vulgaris-leucoagglutinin. J Comp Neurol 296:179–203.

Xavier SM, Barbosa CO, Barros DO, Silva RF, Oliveira AA, Freitas RM (2007) Vitamin C antioxidant effects in hippocampus of adult Wistar rats after seizures and status epilepticus induced by pilocarpine. Neurosci Lett 420:76–79.

Yaari Y, Yue C, Su H (2007) Recruitment of apical dendritic T-type Ca2+ channels by backpropagating spikes underlies de novo intrinsic bursting in hippocampal epileptogenesis. J Physiol 580:435–450.

Zhang Y, Vilaythong AP, Yoshor D, Noebels JL (2004) Elevated thalamic low-voltage-activated currents precede the onset of absence epilepsy in the SNAP25-deficient mouse mutant coloboma. J Neurosci 24:5239–5248.